Published in "Physical Review A 88(1): 012508, 2013"
which should be cited to refer to this work.

Atomic magnetic resonance induced by amplitude-, frequency-, or polarization-modulated light

Z. D. Grujić and A. Weis
Physics Department, University of Fribourg, CH-1700, Fribourg, Switzerland

In recent years diode laser sources have become widespread and reliable tools in magneto-optical spectroscopy. In particular, laser-driven atomic magnetometers have found a wide range of practical applications. More recently, so-called magnetically silent variants of atomic magnetometers have been developed. While in conventional magnetometers the magnetic resonance transitions between atomic sublevels are phase-coherently driven by a weak oscillating magnetic field, silent magnetometers use schemes in which either the frequency or the amplitude of the light beam is modulated. Here we present a theoretical model that yields algebraic expressions for the parameters of the multiple resonances that occur when either amplitude-, frequency-, or polarization-modulated light of circular polarization is used to drive the magnetic resonance transition in a transverse magnetic field. The relative magnitudes of the resonances that are observed in the transmitted light intensity at harmonic m of the Larmor frequency ω_L (either by DC or phase sensitive detection at harmonics q of the modulation frequency $\omega_{\rm mod}$) of the transmitted light are expressed in terms of the Fourier coefficients of the modulation function. Our approach is based on an atomic multipole moment representation that is valid for spin-oriented atomic states with arbitrary angular momentum F in the low light power limit. We find excellent quantitative agreement with an experimental case study using (square-wave) amplitude-modulated light.

I. INTRODUCTION

Magneto-optical spectroscopy of spin-polarized atomic vapors has received a renewed interest thanks to the development of solid-state diode lasers. A comprehensive review of of methods and applications of magneto-optical spectroscopy has been given by Budker *et al.* [1]. One of the most prominent applications of spin-polarized atomic vapors prepared by optical pumping with polarized resonance radiation is atomic magnetometry [2]. Introduced using discharge lamp pumping, atomic magnetometry has received new interest when diode lasers replaced the lamps [3]. Laser pumping has the distinct advantage of allowing multiple sensor arrays to be operated by a single light source [4,5] and allows new (magnetically silent) approaches to magnetometry.

Early magnetometers inferred the magnetometry signal of interest directly from the current of a photodetector monitoring the power of the light traversing the atomic medium. Such magnetometers suffer from low-frequency noise, and the signal to noise ratio, and hence the sensitivity of magnetometers, can be considerably enhanced by using phase-sensitive detection of the photocurrent. Such lock-in detection requires the application of a suitable modulation to the light-atom interaction. In the so-called M_x-magnetometer scheme [6,7] the modulation is achieved by a weak magnetic field that oscillates at the Larmor frequency and that coherently drives the magnetization associated with the atomic spin polarization around the magnetic field. The M_x-magnetometer is an implementation of optically detected magnetic resonance (ODMR), since the driven spin precession consists, in a quantum picture, of magnetic resonance transitions between magnetic sublevels that are driven by the oscillating field.

In recent years several approaches to so-called magnetically silent (or all-optical) modes of magnetometer operation have been put forward. These schemes circumvent the application of the oscillating magnetic field, whose implementation may pose technical problems when the magnetometers are operated in harsh environments, such as in ultrahigh vacuum or in the proximity of high voltage [5]. One of the most successful all-optical magnetometry techniques is frequency-modulated nonlinear magneto-optical rotation (FM-NMOR), in which the coherent spin drive (realized by modulation of the laser frequency) is combined with balanced polarimetric detection [8]. Amplitude modulation (AM) of the laser intensity is another variant of all optical magnetometry. It has been implemented in combination with balanced polarimetric detection [9] and by using direct power monitoring [10]. The fact that amplitude modulated resonance light can drive magnetic resonance transitions in the atomic ground state had already been demonstrated by Bell and Bloom, both with circularly [11] and with linearly [12] polarized light. Do note, however, that those early experiments did not use phase-sensitive detection. Yet another, to our knowledge little-explored, modulation scheme involves the resonant modulation of the laser polarization. Only a few examples of polarization modulation have been discussed in the literature [13–15]. Below we will refer to polarization modulation as Stokes modulation (SM) (since the acronym PM often refers to phase modulation in the literature).

In this paper we derive algebraic expressions for the magnetic resonance spectra of atomic vapors driven by FM-, AM-, or SM-modulated circularly polarized laser light (modulation frequency $\omega_{\rm mod}$). We analyze the temporal structure of the photodetector signal monitoring the light power after the atomic medium and identify resonant signals modulated at harmonics $q\,\omega_{\rm mod}$ of the modulation frequency as well as an unmodulated spectrum of resonances. When demodulated by a lock-in amplifier tuned to an arbitrary harmonic q of $\omega_{\rm mod}$, the magnetic-field-dependent in-phase and quadrature spectra (for a fixed modulation frequency) show an infinite number of absorptive and dispersive Lorentzian resonances located at

multiples $m\,\omega_L$ of the Larmor frequency. We present algebraic expressions that relate the q- and m-dependent amplitudes of these resonances to the Fourier coefficients of the modulation function. Our results are based on an atomic multipole moment approach and are thus applicable to atomic ground states with an arbitrary angular momentum F. The obtained results are valid only in the low light power limit, i.e., in the range where the signal amplitudes grow quadratically with the incident power P_0. In an experimental case study using amplitude modulation (AM) in the low power limit we find an excellent agreement between experimental and theoretical spectra.

Spectra for frequency-modulated (FM) linearly polarized light with polarimetric detection have previously been modeled for a $J = 1$ to $J = 0$ transition using an algebraic density matrix formalism [16]. We are not aware of a related theoretical treatment for AM- or SM-magnetic resonance signals.

II. OPTICALLY INDUCED MAGNETIC RESONANCE

Conventional magnetic resonance is a process in which the orientation of the spin polarization $\vec{S} = \langle \vec{F} \rangle$ of an ensemble of paramagnetic particles (electron, nuclei, atoms) is changed by a resonant interaction of the associated magnetization $\vec{M} = \langle \vec{\mu} \rangle \propto \vec{S}$ with a magnetic field $\vec{b}_1(t)$ oscillating at frequency $\omega_{\rm rf}$. In the case of the atomic ensembles treated here, $\vec{F}$ denotes to the total atomic angular momentum.

In classical terms, the orientation change of $\vec{S}$ is a Larmor precession at frequency $\omega_L \propto |\vec{B}_0|$, driven by the torque $\langle \vec{\mu} \rangle \times \vec{b}_1$. Magnetic resonance occurs when $\omega_{\rm rf}$ matches ω_L. In quantum mechanical terms, magnetic resonance is described in terms of magnetic dipole transitions between the magnetic sublevels $|nL_J, F, m_F\rangle$ of the atom [Fig. 1(a)], and the transition dynamics are determined by the Hamiltonian $H = -\vec{\mu} \cdot \vec{b}_1(t)$, with matrix elements [17]

$$\langle F, m_F' | H | F, m_F \rangle \propto \langle nL_J, F, m_F' | \vec{\mu} | nL_J, F, m_F \rangle \cdot \vec{b}_1(t). \tag{1}$$

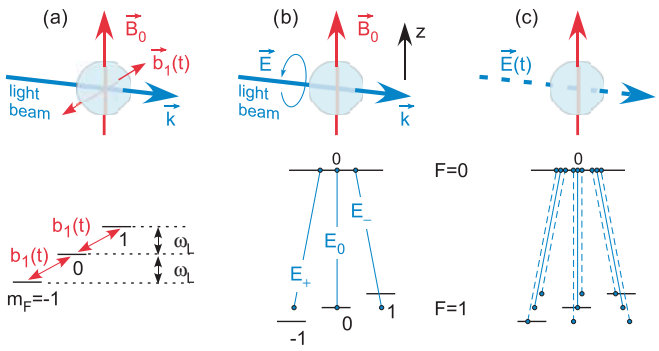

FIG. 1. (Color online) (a) Conventional magnetic resonance: a time-varying field $\vec{b}_1(t)$ induces transitions between magnetic sublevels whose energies are split by the static field $\vec{B}_0$. (b) The light beam serves to prepare the spin orientation and to detect the magnetic resonance transition. $\sigma_\pm$- and π-polarized components of an unmodulated circularly polarized light field with quantization axis along $\vec{B}_0$. (c) Same situation as in (b) when each polarization component (solid lines) acquires sidebands (dashed lines) due to amplitude modulation that induce the sublevel transitions.

For $\Delta L = 0$ transitions, parity conservation requires the operator driving the transitions to be parity even, i.e., invariant under space inversion, which is obeyed by $\vec{\mu}$.

Bell and Bloom have shown [11] that an intensity-modulated resonant light field with circular polarization induces magnetic resonance transitions in an atomic ground state when the modulation frequency $\omega_{\rm mod}$ matches the ground state's Larmor frequency ω_L in a transverse external magnetic field $\vec{B}_0$. The fact that an oscillating electric field can drive $\Delta L = 0$, $\Delta F = 0$ magnetic resonance transitions seems to be in contradiction with the requirement of parity conservation. However, the light-induced magnetic resonance transitions can be understood in terms of parity-conserving second-order processes mediated by the interaction Hamiltonian $H = -\vec{d} \cdot \vec{E}(t)$, as follows. Consider first an *unmodulated* circularly polarized light beam, that excites an atomic $F = 1 \rightarrow F' = 0$ transition, in which the ground-state degeneracy is lifted by a transverse magnetic field $\vec{B}_0$ [Fig. 1(b)]. With the quantization axis along $\hat{B}_0$, the circularly polarized optical field (oscillating at ω) is given by

$$\vec{E} = \sum_q E_q \hat{e}_q = E_0 \sum_q a_q \hat{e}_q = E_0 \left(\frac{1}{2}\hat{e}_+ + \frac{1}{\sqrt{2}}\hat{e}_0 + \frac{1}{2}\hat{e}_- \right), \tag{2}$$

where the subscripts $\pm$ and 0 refer to $\sigma_\pm$ and π polarizations, respectively, in a coordinate frame with quantization axis along $\hat{k}$, which drive transitions from all three sublevels. Because of the energy splitting, only the $0 \rightarrow 0$ transition is resonant in the case shown. When the amplitude of the light is modulated at frequency $\omega_{\rm mod}$, its Fourier spectrum acquires sidebands that are offset by $\pm n\omega_{\rm mod}$ from the optical frequency. In Fig. 1(c), we show the carrier E_0, oscillating at the optical frequency ω (solid lines), together with the $n = \pm 1$ sidebands $E_\pm$, oscillating at $\omega \pm \omega_{\rm mod}$ (dashed lines) for the resonant case where $\omega_{\rm mod} = \omega_L$. For simplicity we ignore the higher-order sidebands in the present discussion. These sidebands are responsible for resonances at harmonics of the Larmor frequency (see also discussion in Sec. 4D of Ref. [14]).

With this simplification, the carrier $\vec{E}_0$, together with one of the sidebands $\vec{E}_{\pm 1}$ resonantly drive $\Delta m_F = \pm 1$ transitions between adjacent sublevels. The matrix elements of this second-order process can be written in terms of an effective Hamiltonian [18] as

$$\langle F, m_F' | H_{\rm eff} | F, m_F \rangle \propto \sum_{q,q'=0,\pm 1} (-1)^{q+q'} \langle F, m_F' | d_{-q'}\, d_{-q} | F, m_F \rangle\, E_{q'} E_q. \tag{3}$$

The bilinear form of the dipole operators d_q in (3) ensures that the matrix elements are parity even and that the effective Hamiltonian $H_{\rm eff}$ indeed conserves parity.

Selection rules and relative line strengths for transitions mediated by (3) were derived in Ref. [18]. Moreover, one finds that the two $\sigma_\pm$ polarized components in Fig. 1(c) cannot drive $\Delta m_F = 2$ transitions because of destructive quantum interference, thus respecting the conventional $\Delta m_F = 0, \pm 1$ selection rule for magnetic resonance transitions. However, when using modulated *linearly polarized* light and a field $\vec{B}_0$, perpendicular to the light polarization, the two sidebands

lead to constructive interference, thereby allowing $\Delta m_F = 2$ transitions to occur. In this way Bell and Bloom were able to observe the "forbidden" $\Delta m_F = 2$ magnetic resonance transitions [12] using amplitude-modulated *linearly*polarized light.

Alzetta *et al.* [19] devised an elegant method that allowed the photographic visualization of Bell-Bloom type magnetic resonance processes induced by polychromatic light fields. The method has since become known as coherent population trapping (CPT). We stress an important aspect of CPT spectroscopy: Since in the ground state the magnetic sublevel coherences excited by bichromatic or polychromatic light fields may be very long lived (up to seconds), one has to ensure that the individual Fourier components of the exciting light field have a phase coherence which lives at least as long as the atomic coherence. With Fourier components produced as sidebands by a modulation technique, the phase coherence is determined by the phase stability of the generator driving the modulator. However, when the multimode light field is produced by a superposition of independent laser sources, special care has to be taken to actively phase lock the individual optical fields.

III. MAGNETIC RESONANCE WITH CIRCULARLY-POLARIZED MODULATED LIGHT

A. Experimental geometry

Figure 2 shows the geometry of the experiments discussed in this paper. A circularly polarized laser beam, resonant with an $F \rightarrow F'$ transition, traverses an atomic vapor cell of length L that is exposed to a transverse static magnetic field $\vec{B}_0$. The power $P(t)$ of the light transmitted through the cell is measured by a photodetector. For suppression of technical noise, one may wish to use a balanced polarimeter detecting alterations of the light polarization rather than merely detecting the light power. Such extensions of the method will not be addressed here.

We will discuss three distinct experiments, in which a given property, viz., the power $P_0(t)$, the frequency detuning $\delta\omega(t)$ from the atomic transition, or the helicity $\xi(t)$ of the incident light field is subject to a periodic modulation at frequency $\omega_{\rm mod}$. The modulated property will imprint a characteristic periodic modulation at $\omega_{\rm mod}$, or harmonics q thereof, onto the power of the transmitted beam, with amplitude(s) and phase shift(s) that depend on the detuning of the Larmor frequency

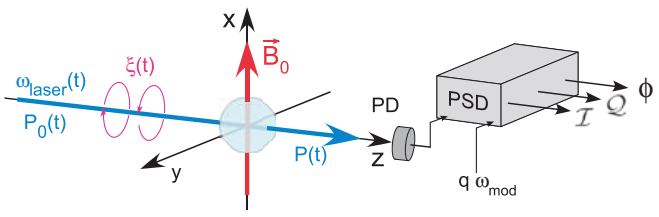

FIG. 2. (Color online) Experiments addressed in this paper. A circularly polarized resonant light beam traverses an atomic medium exposed to a static magnetic field $\vec{B}_0$. Either the power P_0, the frequency $\omega_{\rm laser}$, or the polarization (helicity) ξ of the light is modulated at frequency $\omega_{\rm mod}$ and a phase sensitive detector (PSD), tuned to $q\omega_{\rm mod}$, extracts the in-phase component ($\mathcal{I}$), the quadrature component ($\mathcal{Q}$), and the phase (ϕ) of the signal from the photodiode (PD) detecting the transmitted modulated power $P(t)$.

$\omega_L = \gamma_F\,|\vec{B}_0|$ from $q\,\omega_{\rm mod}$, where γ_F is the gyromagnetic ratio of the polarized ground state F.

In the experiments, the time dependent photodetector signal $P(t)$ is analyzed by a phase-sensitive detector (PSD), referenced to $\omega_{\rm mod}$ or its q-th harmonic. At each demodulation frequency q $\omega_{\rm mod}$, one observes a series of resonances at multiples $m\,\omega_L$ (m, arbitrary integer) of the Larmor frequency. The aim of the present paper is the derivation of algebraic expressions for the amplitudes $a_{q,m}$ and $d_{q,m}$ of the in-phase and quadrature components of $P(t)$.

B. Light transmission through a spin-polarized vapor

The light power P transmitted by an unpolarized optically thin atomic vapor of length L is given by

$$P = P_0\, e^{-\kappa(\delta\omega)\,L} \approx P_0 - P_0\,\kappa(\delta\omega)\,L, \tag{4}$$

where

$$\kappa(\delta\omega) = \kappa_0\, D(\delta\omega) \tag{5}$$

is the optical absorption coefficient, parametrized in terms of the peak absorption coefficient κ_0 and a spectral line-shape function $D(\delta\omega)$, typically a Doppler or Voigt profile with $D(0) = 1$, that depends on the detuning $\delta\omega = \omega_{\rm laser} - \omega_0$ of the laser frequency $\omega_{\rm laser}$ from the atomic resonance frequency ω_0.

When the medium is spin polarized, the peak absorption coefficient for light with circular polarization σ_ξ has to be replaced by

$$\kappa_0 \rightarrow \kappa_0[1 - \alpha_{F,F'}\,\xi\,S_z - \beta_{F,F'}\,A_{zz}], \tag{6}$$

where

$$S_z = \frac{1}{F}\sum_{m_F=-F}^{F} m_F\, p_{m_F} \tag{7}$$

and

$$A_{zz} = \frac{1}{F(2F-1)}\sum_{m_F=-F}^{F}\left[3m_F^2 - F(F+1)\right]\, p_{m_F} \tag{8}$$

are the vector polarization (orientation) and tensor polarization (alignment) of the medium, respectively, with p_{m_F} being the normalized sublevel populations $\sum p_{m_F} = 1$. Both S_z and A_{zz} are defined here to be normalized to unity when the system is in the stretched state defined by $p_{m_F} = \delta_{m_F,F}$. The coefficients $\alpha_{F,F'}$ and $\beta_{F,F'}$ depend on the angular momenta F, F' of the states coupled by the optical transition.

Optical pumping with circularly polarized light produces both orientation and alignment in the ground state. In order not to overcharge the present paper we will consider only orientation contributions by setting $\beta_{F,F'} = 0$. As discussed at the end of the paper, we have in fact observed weak signal components that can be assigned to alignment contributions. Since these components are spectrally resolved from the orientation contributions, they will not be addressed here. With the above restrictions the transmitted power is given by

$$P = [1 - \kappa_0 L\, D(\delta\omega)]\;P_0 + \alpha\kappa_0 L\, D(\delta\omega)\,\xi\, S_z\, P_0. \tag{9}$$

We will not address the dependence of $\alpha_{F,F'}$ on F and F', and drop the indices in consequence. The combinations $\kappa_0 L$ and

$\alpha\kappa_0 L$ can be seen as experimental parameters, which can be determined empirically.

C. Modulation schemes

We address the following three modulation schemes.

(i) Amplitude modulation (AM): The laser frequency is set to resonance, $D(\delta\omega = 0) = 1$, the polarization is fixed to $\xi = +1$, and the incident light power is modulated by an arbitrary periodic time dependent function according to $P_0(t) = P_0\, f^{\rm AM}_{\omega_{\rm mod}}(t)$. The corresponding time dependence of the detected power then reads

$$P^{\rm AM}(t) = (1-\kappa_0 L)\; P_0(t) + \alpha\kappa_0 L\, S_z^{\rm AM}(t)\, P_0(t) \tag{10}$$

$$= (1-\kappa_0 L)\; P_0\, f^{\rm AM}_{\omega_{\rm mod}}(t) + \alpha\kappa_0 L\, P_0\, S_z^{\rm AM}(t) \times f^{\rm AM}_{\omega_{\rm mod}}(t) \tag{11}$$

$$\equiv A^{\rm AM} + B^{\rm AM}\, f^{\rm AM}_{\omega_{\rm mod}}(t) + C^{\rm AM}\, S_z^{\rm AM}(t) \times f^{\rm AM}_{\omega_{\rm mod}}(t). \tag{12}$$

(ii) Frequency modulation (FM): The incident power is fixed to P_0, the helicity of the light polarization is fixed to $\xi = +1$, and the laser detuning $\delta\omega(t)$ is periodically modulated. The corresponding time dependence of the detected power reads

$$P^{\rm FM}(t) = [1-(\kappa_0 L)\, D(\delta\omega(t))]\; P_0 + (\alpha\,\kappa_0 L)\, P_0\, S_z^{\rm FM}(t) \times D(\delta\omega(t)). \tag{13}$$

The modulation function can be modeled by replacing $D(\delta\omega(t))$ by a periodic function $f^{\rm FM}_{\omega_{\rm mod}}(t)$, with $0 \leqslant f^{\rm FM}_{\omega_{\rm mod}} \leqslant 1$. With this choice, the transmitted power can be written as

$$P^{\rm FM}(t) = P_0 - (\kappa_0 L\; P_0)\, f^{\rm FM}_{\omega_{\rm mod}}(t) + (\alpha\,\kappa_0 L\; P_0)\, S_z^{\rm FM}(t) \times f^{\rm FM}_{\omega_{\rm mod}}(t) \tag{14}$$

$$\equiv A^{\rm FM} + B^{\rm FM}\, f^{\rm FM}_{\omega_{\rm mod}}(t) + C^{\rm FM}\, S_z^{\rm FM}(t) \times f^{\rm FM}_{\omega_{\rm mod}}(t). \tag{15}$$

(iii) Polarization modulation (SM): The laser frequency is set to resonance, $D(\delta\omega = 0) = 1$, the incident power is fixed to P_0, and the helicity (degree of circular polarization) of the light is periodically modulated as $\xi(t) = f^{\rm SM}_{\omega_{\rm mod}}(t)$, with $|f^{\rm SM}_{\omega_{\rm mod}}| \leqslant 1$. The corresponding time dependence of the detected power reads

$$P^{\rm SM}(t) = (1-\kappa_0 L)\, P_0 + (\alpha\,\kappa_0 L\; P_0)\, S_z^{\rm SM}(t) \times f^{\rm SM}_{\omega_{\rm mod}}(t) \tag{16}$$

$$\equiv A^{\rm SM} + B^{\rm SM}\, f^{\rm SM}_{\omega_{\rm mod}}(t) + C^{\rm SM}\, S_z^{\rm SM}(t) \times f^{\rm SM}_{\omega_{\rm mod}}(t). \tag{17}$$

We see that all three types of experiments (TOE) can be parametrized in terms of distinct time-independent and time-dependent terms of the general form

$$P^{\rm TOE}(t) = A^{\rm TOE} + B^{\rm TOE}\, f^{\rm TOE}_{\omega_{\rm mod}}(t) + C^{\rm TOE}\, S_z^{\rm TOE}(t)\, f^{\rm TOE}_{\omega_{\rm mod}}(t). \tag{18}$$

TABLE I. Characteristic parameters $A^{\rm TOE}$, $B^{\rm TOE}$, and $C^{\rm TOE}$ for experiments with amplitude- (AM), frequency- (FM), and polarization-modulated (SM) light, respectively. The last column gives the lower and upper bounds of the modulation functions $f^{\rm TOE}_{\omega_{\rm mod}}$(t) for achieving a maximal contrast of the system's response.

TOE	$A^{\rm TOE}$	$B^{\rm TOE}$	$C^{\rm TOE}$	$f^{\rm TOE}_{\omega_{\rm mod}}$(t)
AM	0	$(1-\kappa_0 L)\; P_0$	$\alpha\,\kappa_0 L\; P_0$	$f^{\rm AM}_{\omega_{\rm mod}} \in [0,1]$
FM	P_0	$-\kappa_0 L\; P_0$	$\alpha\,\kappa_0 L\; P_0$	$f^{\rm FM}_{\omega_{\rm mod}} \in [0,1]$
SM	$(1-\kappa_0 L)\; P_0$	0	$\alpha\,\kappa_0 L\; P_0$	$f^{\rm SM}_{\omega_{\rm mod}} \in [-1,1]$

The parameters A, B, C for amplitude-, frequency-, and polarization-modulation are summarized in Table I.

We note the following facts:

(i) The time-independent term $A^{\rm TOE}$ gives no contribution to the lock-in signals.

(ii) The term $B^{\rm TOE}$ has the same Fourier spectrum as the time-dependent modulation, but contains no magnetic-field-dependent quantities. In AM and FM experiments it will lead to a field-independent background that is, for an optically thin medium, $\kappa_0 L \ll 1$, substantially larger in AM experiments than in FM experiments, while in SM experiments it is absent.

(iii) The $C^{\rm TOE}$ term leads to a richer spectrum because of the mixing of frequencies of its two time-dependent contributions $S_z(t)$ and $f^{\rm TOE}_{\omega_{\rm mod}}(t)$. We note that only the $C^{\rm TOE}$ term depends—via $S_z(t)$—on the magnetic field, while the $A^{\rm TOE}$ and $B^{\rm TOE}$ terms form a signal background that influences the contrast and the signal to noise ratio of the magnetic resonance structures.

In Sec. IV we will first derive algebraic expressions that relate the time-dependent spin orientation $S_z^{\rm TOE}(t)$ to the specific drive function $f^{\rm TOE}_{\omega_{\rm mod}}(t)$, and in Sec. V we will then derive and discuss the complete Fourier spectra of the signals $P^{\rm TOE}(t)$.

IV. SPIN ORIENTATION $S_z(t)$ UNDER PERIODIC MODULATION

As stated above, we will not address alignment contributions to the atomic polarization and describe the latter only in terms of its vector polarization (orientation) $\vec{S}$. The dynamics of $S_z(t)$, i.e., the only polarization component that contributes to the signals, is governed by the Bloch equations

$$\dot{\vec{S}} = \vec{S} \times \vec{\omega}_L - \gamma\, \vec{S} + \Gamma_p^{\rm TOE}(t)\, \hat{k}, \tag{19}$$

whose components read

$$\dot{S}_x = -\gamma\, S_x \tag{20}$$

$$\dot{S}_y = +\omega_L\, S_z - \gamma\, S_y \tag{21}$$

$$\dot{S}_z = -\omega_L\, S_y - \gamma\, S_z + \Gamma_p^{\rm TOE}(t), \tag{22}$$

where we have assumed that the longitudinal and transverse relaxation rates are identical $\gamma_1 = \gamma_2 \equiv \gamma$, and where $\Gamma_p^{\rm TOE}(t)$ is a source term that describes the rate at which longitudinal orientation S_z is produced by optical pumping. We note that the pumping rate $\Gamma_p(t)$ is proportional to the product of the incident power P_0, the light helicity ξ, and the optical line shape $D(\delta\omega)$. The modulation of any of these quantities thus yields a modulation of the pumping (and probing) rate, that

can be parametrized as

$$\Gamma_p^{\mathrm{TOE}}(t) = \gamma_p \, f_{\omega_{\mathrm{mod}}}^{\mathrm{TOE}}(t), \tag{23}$$

where $f_{\omega_{\mathrm{mod}}}^{\mathrm{TOE}}(t)$ is the modulation function which varies periodically within the bounds listed in Table I. The pumping rate amplitude can be related to the light power P_0 (or the light intensity I_A) by introducing a saturation parameter G, defined as

$$G \equiv \frac{\gamma_p}{\gamma} \equiv \frac{P_0}{P_s} \equiv \frac{I}{I_s}, \tag{24}$$

where P_s and I_s are the saturation power and saturation intensity, respectively.

We note that the Bloch equations above, and hence the solutions below, are only valid in the low-power approximation $P_0 \ll P_S$, i.e., $\gamma_p \ll \gamma$, which expresses the fact that less than one optical pumping (absorption/fluorescence) cycle occurs during the lifetime γ^{-1} of the ground-state polarization.

A. Monochromatic modulation

Using Wolfram MATHEMATICA 8.0 [20], one can show that the Bloch equation for $S_z(t)$ driven by a monochromatic modulation around a DC offset value

$$\Gamma_p^{\mathrm{AM,FM}}(t) = \frac{\gamma_p}{2}\left[1 + \cos\left(\omega_{\mathrm{mod}} t\right)\right]. \tag{25}$$

has a time-dependent solution of the form

$$S_z^{\mathrm{AM,FM}}(t) = \frac{\gamma_p}{2}\left[T(t) + R(t)\right], \tag{26}$$

with

$$\begin{aligned} T^{\mathrm{AM,FM}}(t) = &\left[\frac{2\,\omega_L}{\omega_L^2+\gamma^2} + \frac{\omega_L-\omega_{\mathrm{mod}}}{(\omega_L-\omega_{\mathrm{mod}})^2+\gamma^2} + \frac{\omega_L+\omega_{\mathrm{mod}}}{(\omega_L+\omega_{\mathrm{mod}})^2+\gamma^2}\right]\sin(\omega_L t)\, e^{-\gamma t} \\ &- \left[\frac{2\,\gamma}{\omega_L^2+\gamma^2} + \frac{\gamma}{(\omega_L-\omega_{\mathrm{mod}})^2+\gamma^2} + \frac{\gamma}{(\omega_L+\omega_{\mathrm{mod}})^2+\gamma^2}\right]\cos(\omega_L t)\, e^{-\gamma t}, \end{aligned} \tag{27}$$

$$\begin{aligned} R^{\mathrm{AM,FM}}(t) = &\frac{2\,\gamma}{\omega_L^2+\gamma^2} + \left[\frac{\gamma}{(\omega_{\mathrm{mod}}-\omega_L)^2+\gamma^2} + \frac{\gamma}{(\omega_{\mathrm{mod}}+\omega_L)^2+\gamma^2}\right]\cos(\omega_{\mathrm{mod}} t) \\ &+ \left[\frac{\omega_{\mathrm{mod}}-\omega_L}{(\omega_{\mathrm{mod}}-\omega_L)^2+\gamma^2} + \frac{\omega_{\mathrm{mod}}+\omega_L}{(\omega_{\mathrm{mod}}+\omega_L)^2+\gamma^2}\right]\sin(\omega_{\mathrm{mod}} t). \end{aligned} \tag{28}$$

The function $T^{\mathrm{AM,FM}}(t)$ is a damped transient, so that for $t \gg \gamma^{-1}$ $S_z(t)$ shows a steady-state oscillation given by

$$S_z^{\mathrm{AM,FM}}(t) = \frac{\gamma_p}{2}\, R(t)^{\mathrm{AM,FM}} \tag{29}$$

$$= \frac{G}{2}\mathcal{H}(\omega_L) + \frac{G}{2}\left[\mathcal{A}(\omega_L) + \mathcal{A}(-\omega_L)\right] \times \cos(\omega_{\mathrm{mod}} t) \tag{30}$$

$$+ \frac{G}{2}\left[\mathcal{D}(\omega_L) + \mathcal{D}(-\omega_L)\right]\sin(\omega_{\mathrm{mod}} t), \tag{31}$$

with resonance line shapes

$$\mathcal{H}(\omega_L) = \frac{2\,\gamma^2}{\omega_L^2+\gamma^2} \tag{32}$$

$$\mathcal{A}(\omega_L) = \frac{\gamma^2}{(\omega_{\mathrm{mod}}-\omega_L)^2+\gamma^2} \tag{33}$$

$$\mathcal{D}(\omega_L) = \frac{\gamma\,(\omega_{\mathrm{mod}}-\omega_L)}{(\omega_{\mathrm{mod}}-\omega_L)^2+\gamma^2}. \tag{34}$$

The spin polarization thus contains an unmodulated DC Lorentzian (Hanle) resonance centered at $\omega_L = 0$, as well as absorptive and dispersive Lorentzians, centered at $\omega_L = \pm\omega_{\mathrm{mod}}$.

We note that the DC term in the pumping rate (25) occurs only in the AM and FM schemes, while the SM modulation function (normalized to the same peak-peak modulation amplitude)

$$\Gamma_p^{\mathrm{SM}}(t) = \frac{\gamma_p}{2}\cos\left(\omega_{\mathrm{mod}} t\right) \tag{35}$$

has no DC part.

The steady-state Bloch oscillations in that case are given by

$$\begin{aligned} S_z^{\mathrm{SM}}(t) = \frac{G}{2}\{&\left[\mathcal{A}(\omega_L) + \mathcal{A}(-\omega_L)\right]\cos(\omega_{\mathrm{mod}} t) \\ &+ \left[\mathcal{D}(\omega_L) + \mathcal{D}(-\omega_L)\right]\sin(\omega_{\mathrm{mod}} t)\}, \end{aligned} \tag{36}$$

and show no Hanle resonance in the unmodulated DC signal.

B. Arbitrary periodic modulation

We consider next an arbitrary symmetric ($g_m = g_{-m}$) periodic modulation that can be represented in terms of its cosine-Fourier series

$$\Gamma_p^{\mathrm{TOE}}(t) = \gamma_p \, f_{\omega_{\mathrm{mod}}}^{\mathrm{TOE}}(t) = \gamma_p \sum_{m=-\infty}^{\infty} g_m \cos\left(m\,\omega_{\mathrm{mod}} t\right). \tag{37}$$

Since the Bloch equations are linear in γ_p, they can be solved for each Fourier component $\cos(m\,\omega_{\mathrm{mod}} t)$ independently,

yielding

$$S_z^{(m)}(t) = g_m\, G\, \{[\mathcal{A}_m(\omega_L) + \mathcal{A}_m(-\omega_L)]\cos(m\omega_{\rm mod}t) + [\mathcal{D}_m(\omega_L) + \mathcal{D}_m(-\omega_L)]\sin(m\omega_{\rm mod}t)\}$$
$$= g_m\, G\, \{[\mathcal{A}_m(\omega_L) + \mathcal{A}_{-m}(\omega_L)]\cos(m\omega_{\rm mod}t) + [\mathcal{D}_m(\omega_L) - \mathcal{D}_{-m}(\omega_L)]\sin(m\omega_{\rm mod}t)\}\,, \tag{38}$$

with

$$\mathcal{A}_m(\omega_L) = \frac{\gamma^2}{(m\omega_{\rm mod} - \omega_L)^2 + \gamma^2}, \tag{39}$$

$$\mathcal{D}_m(\omega_L) = \frac{\gamma(m\omega_{\rm mod} - \omega_L)}{(m\omega_{\rm mod} - \omega_L)^2 + \gamma^2}. \tag{40}$$

Note that we have replaced the experiment indicating superscript TOE on $S_z(t)$ by the order m of the resonance behavior of the Fourier coefficient, and have added the subscript m to $\mathcal{A}(\omega_L)$ and $\mathcal{D}(\omega_L)$ to denote the Fourier component at $m\omega_{\rm mod}$. By a proper choice of the coefficients g_m, the expressions can be applied to all three types of experiments.

Summing all Fourier components, we find that the time-dependent spin polarization is given by

$$S_z(t) = \sum_{m=-\infty}^{\infty} S_z^{(m)}(t) = 2\,G \sum_{m=-\infty}^{\infty} g_m \big[\mathcal{A}_m(\omega_L) \times \cos(m\omega_{\rm mod}t) + \mathcal{D}_m(\omega_L)\, \sin(m\omega_{\rm mod}t)\big]. \tag{41}$$

The factor 2 in the last expression originates from the symmetries $\mathcal{A}_{-m} = \mathcal{A}_m$ and $\mathcal{D}_{-m} = -\mathcal{D}_m$ of the line-shape functions. The Hanle resonance of (31) is now explicitly contained as the $m = 0$ term in the sum since $\mathcal{H} = \mathcal{A}_0 + \mathcal{A}_{-0}$.

V. THE LOCK-IN SIGNALS

In Appendix A we show that the transmitted power (photodiode signal) contains time-independent and time-dependent contributions

$$P^{\rm TOE}(t) = \mathcal{B}_{\rm DC}^{\rm TOE} + \sqrt{2}\sum_{q=1}^{\infty} \mathcal{I}_{\rm q}^{\rm TOE}\, \cos(q\,\omega_{\rm mod}t) + \sqrt{2}\sum_{q=1}^{\infty} \mathcal{Q}_{\rm q}^{\rm TOE}\, \sin(q\,\omega_{\rm mod}t)\,. \tag{42}$$

The time-independent (DC) signal is given by

$$\mathcal{B}_{\rm DC}^{\rm TOE} = A^{\rm TOE} + g_0\, B^{\rm TOE} + G\, C^{\rm TOE} \sum_{m=-\infty}^{\infty} g_m^2\, \mathcal{A}_m(\omega_L), \tag{43}$$

which represents an infinite series of absorptive Lorentzians, centered at $\omega_L = m\,\omega_{\rm mod}$, respectively, that are superposed on a field-independent background $A^{\rm TOE} + g_0\, B^{\rm TOE}$. The constants $A^{\rm TOE}$, $B^{\rm TOE}$, and $C^{\rm TOE}$ are given in Table I for the different types of experiments. We note that for TOE = AM, the $m = 0$ term represents the magnetic resonance described in the early work of Bell and Bloom [11].

The photodiode signal further contains (periodic) time-dependent components that oscillate in-phase and in quadrature with the fundamental and higher harmonics of the modulation frequency $\omega_{\rm mod}$. $\mathcal{I}_{\rm q}^{\rm TOE}(\omega_L)$ and $\mathcal{Q}_{\rm q}^{\rm TOE}(\omega_L)$ represent the rms amplitudes of these signals, when extracted by a lock-in amplifier (Fig. 2) referenced by $\cos q\omega_{\rm mod}$, respectively,

$$\mathcal{I}_{\rm q}^{\rm TOE}(\omega_L) = h_q + \sum_{m=-\infty}^{\infty} a_{q,m}\, \mathcal{A}_m(\omega_L), \tag{44}$$

with

$$h_q = \sqrt{2}\, g_q\, B^{\rm TOE} \quad \text{and}$$
$$a_{q,m} = \sqrt{2}\, G\, C^{\rm TOE}\, g_m\, (g_{q-m} + g_{q+m}). \tag{45}$$

The corresponding quadrature signals read

$$\mathcal{Q}_{\rm q}^{\rm TOE} = \sum_{m=-\infty}^{\infty} d_{q,m}\mathcal{D}_m(\omega_L), \quad \text{with}$$
$$d_{q,m} = \sqrt{2}\, G\, C^{\rm TOE}\, g_m\, (g_{q-m} - g_{q+m}). \tag{46}$$

At each demodulation harmonic q, one thus observes an infinite series of absorptive and dispersive Lorentzians, centered at $\omega_L = \pm m\,\omega_{\rm mod}$. The absorptive resonances of the in-phase spectrum have amplitudes given by $a_{q,m}$ which are expressed in terms of a type-of-experiment specific constant $C^{\rm TOE}$, the peak optical pumping rate γ_p (itself proportional to the incident laser power P_0), and a simple algebraic function of the Fourier coefficients g_i of the specific modulation function $f^{\rm TOE}(t)$ of similar composition. The quadrature spectrum consists of dispersive Lorentzians of amplitudes $d_{q,m}$.

We note that the in-phase resonance spectrum is superposed on a magnetic-field-independent background of amplitude h_q, which vanishes for polarization modulation (TOE = SM), and is reduced by a factor $\alpha\kappa_0 L$ in FM experiments compared to AM experiments. The quadrature spectrum is background free at all demodulation harmonics and for all three types of experiments. We further note that the in-phase spectrum contains absorptive zero-field ($m = 0$) Hanle resonances at all demodulation harmonics $q\,\omega_{\rm mod}$, which have no dispersive counterparts in the quadrature signals since $d_{q,0} = 0$.

The linear zero crossings at the centers of the dispersive resonances offer a convenient discriminator signal for magnetometers in which active feedback is used to stabilize the Larmor frequency ω_L to the modulation frequency $\omega_{\rm mod}$ (or vice versa).

VI. MAGNETIC RESONANCE INDUCED BY AMPLITUDE MODULATED LIGHT

A. Experiments

In order to illustrate how well Eqs. (44)–(46) describe experimental spectra, we present the result of a case study using amplitude-modulated light. Related experiments were

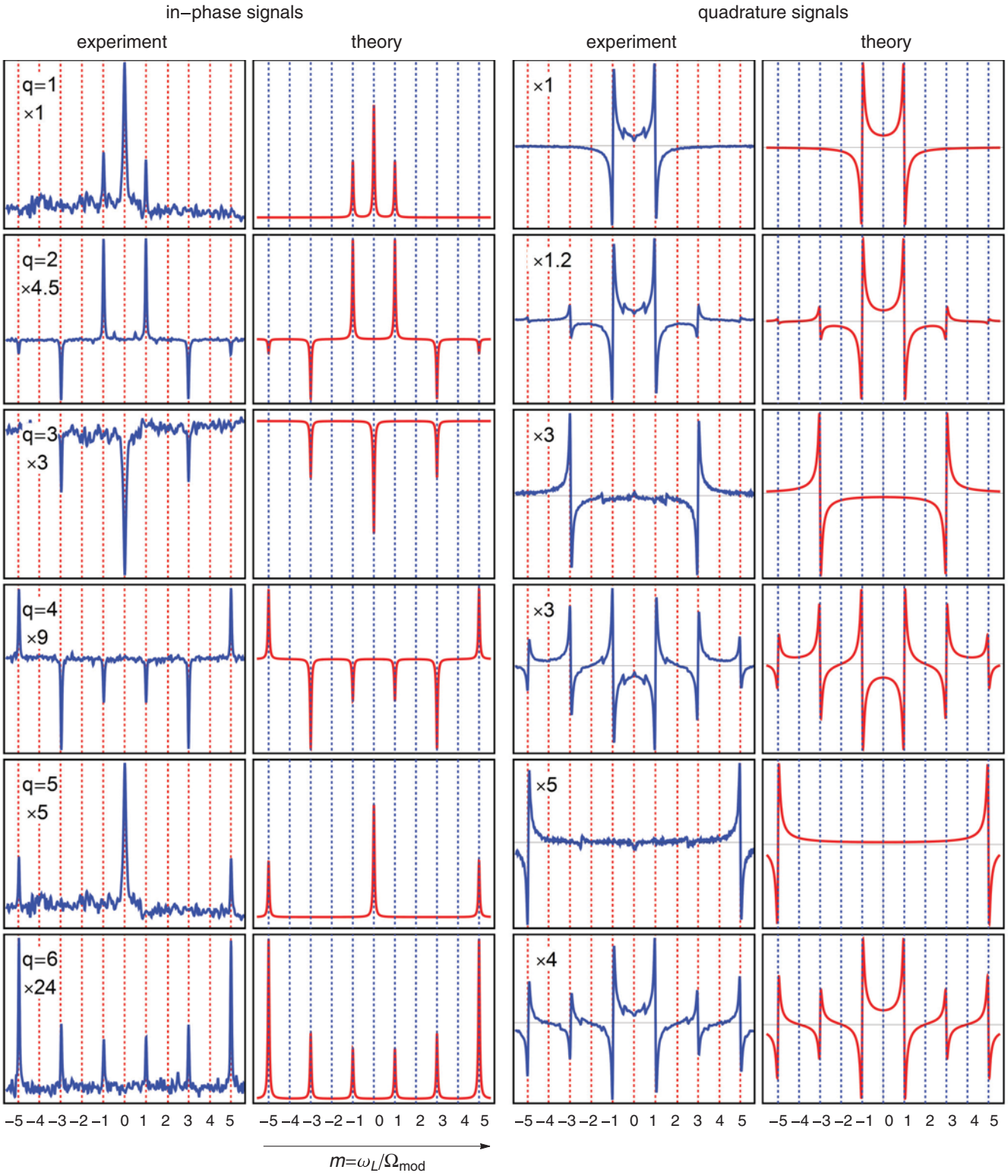

FIG. 3. (Color online) Comparison of experimental and theoretical magnetic resonance spectra excited by amplitude-modulated circularly polarized light (50% duty cycle) in a transverse magnetic field (Larmor frequency ω_L). The modulation frequency $\omega_{\rm mod} = (2\pi)127$Hz was kept constant while the magnetic field was scanned. The magnetic field amplitude is represented in units of the modulation frequency ($m = \omega_L/\omega_{\rm mod}$). The left and right parts of the figure show, respectively, the lock-in extracted in-phase $\mathcal{I}$ and quadrature $\mathcal{Q}$ components of the photocurrent monitoring the transmitted modulated light intensity. The parameter q denotes the harmonic of $\omega_{\rm mod}$ at which the signal was demodulated. In each column, all spectra are normalized to the amplitude of the $q = 1, m = 1$ resonance in that column.

TABLE II. Comparison of theoretical and experimental peak-peak amplitudes $d_{q,m}/d_{1,1}$ of the dispersive resonances in an AM experiment, normalized to the amplitude of the resonance with $q = 1$ and $m = 1$. The row label q refers to the frequency $q\,\omega_{\rm mod}$ at which the signals are demodulated. The column label m denotes the position of the resonances at $\omega_L = \pm m\,\omega_{\rm mod}$.

		$m=1$	2	3	4	5	6
$q=1$	theo.	1	0	0	0	0	0
	exp.	1	0	0	0	0	0
2	theo.	$+16/3\pi = 0.849$	0	$-16/15\pi = -0.170$	0	$-16/105\pi = -0.024$	0
	exp.	+0.844(27)	0	−0.168(5)	0	−0.023(1)	0
3	theo.	0	0	$-1/3 = -0.333$	0	0	0
	exp.	0	0	−0.343(10)	0	0	0
4	theo.	$-32/15\pi = -0.340$	0	$-32/21\pi = -0.243$	0	$+32/45\pi = +0.113$	0
	exp.	−0.348(11)	0	−0.247(8)	0	+0.117(4)	0
5	theo.	0	0	0	0	$+1/5 = 0.200$	0
	exp.	0	0	0	0	+0.205(7)	
6	theo.	$+48/35\pi = +0.218$	0	$+16/27\pi = +0.094$	0	$+48/55\pi = +0.139$	0
	exp.	+0.229(8)	0	+0.095(3)	0	+0.141(5)	0

reported in the literature [9,10]. Our experiments were done in a paraffin-coated Cs vapor cell, using a laser beam whose frequency was actively stabilized to the $4 \to 3$ hyperfine transition of the D_1 line. Following the procedure outlined in Ref. [21], we choose the light power to be sufficiently low ($1.4\mu W$) to ensure the validity of the theoretical model. The experiments were carried out in a threefold μ-metal shield, in which the power of the circularly polarized laser beam traversing the cell was recorded by a photodiode. We used a compact fiber-coupled sensor, similar to the one described in Ref. [22], that contained the polarization optics, the vapor cell and the photodiode, and that was mounted inside of a long solenoid producing the transverse magnetic field.

The laser intensity was given a square-wave on/off modulation with a 50/50 duty cycle using an acousto-optic modulator. The photocurrent was amplified by a transimpedance amplifier and analyzed by a Zurich Instruments (model HF2LI) lock-in amplifier, which allowed the simultaneous extraction of the in-phase and quadrature components at six selected harmonics of its reference frequency.

B. Analysis and discussion

The results are shown in Fig. 3, together with the theoretical prediction based on (44)–(46), evaluated with the Fourier coefficients

$$g_0 = \frac{1}{2} \quad \text{and} \quad g_{k\neq 0} = \frac{1}{\pi}\,\frac{\sin\left(k\,\frac{\pi}{2}\right)}{k} \tag{47}$$

of the symmetric, $f_{\rm mod}(t) = f_{\rm mod}(-t)$, square-wave modulation function. The only posttreatment applied to the recorded data was the subtraction of the DC offset of the in-phase components and the scaling of all experimental data $\mathcal{Q}_q$, and $\mathcal{I}_q$ (after the mentioned offset subtraction) by a *one common* multiplicative factor, chosen such that the theoretical amplitudes of the dispersive resonance in the first harmonic ($q = 1$) spectrum match the amplitudes of the corresponding experimental spectrum. One sees that this single scaling factor yields an excellent agreement between the experimental spectra and the theoretical predictions for the whole range of investigated q and m values.

In Table II we present a quantitative comparison of the predicted and measured peak-peak amplitudes of the dispersive resonances, since the quadrature resonances have a superior signal to noise ratio (SNR). The experimental zero in the Table II means that under our experimental conditions a resonance was not observed. The poorer SNR of the in-phase signals arises from the background signal $B^{\rm TOE}$ that is proportional to the incident laser power P_0, so that power fluctuations of P_0 produce noise on the in-phase components that surpasses the noise on the quadrature components by a factor on the order of $B^{\rm AM}/C^{\rm AM} \approx (\alpha\kappa_0 L)^{-1}$. We note that this excess noise factor reduces to α^{-1} in the case of FM experiments, and that it is unity for SM experiments, since the in-phase components in such experiments are background free.

C. Hanle resonances

As anticipated by the model, zero-field Hanle resonances are only observed on the in-phase spectra. Here we do not attempt to analyze the relative magnitudes of the $\omega_L = 0$ resonance(s) and the resonances with $m \neq 0$, since the widths and amplitudes of the zero-field level crossing resonances are strongly affected by field inhomogeneities, i.e., by residual transverse field components. In the experiments reported here, no effort was made to precisely cancel such transverse components, since the resonances of interest are only marginally affected by such field components.

D. Alignment resonances

The experimental quadrature spectra show small resonant structures at multiples of $\omega_L/2$ (Fig. 3). Our initial guess was that these resonances originate from an imperfect degree of circular polarization, i.e., from a small degree of linear polarization. During completion of the present work we realized that these resonances are due to atomic alignment along the light propagation direction that is produced (and probed) by

the circularly polarized laser beam. It so happens that the production and detection of alignment is very inefficient on the $4 \rightarrow 3$ transition that was chosen for the above case study. Subsequent experiments, not shown here, have shown that these alignment contributions are much more pronounced on the other three hyperfine components of the D_1 line, and that the corresponding resonance amplitudes may even surpass those of the orientation-based signals in some cases. These resonances are a topic for future study.

VII. SUMMARY AND CONCLUSION

We have presented a quantitative algebraic model that describes the features of the complex magnetic resonance patterns that are observed in experiments using synchronous optical pumping with modulated circularly polarized light in a transverse magnetic field. The model considers only contributions from atomic spin orientation (vector polarization), but is general in the sense that it can be applied—with a suitable choice of model parameters—to amplitude-, frequency-, and polarization-modulation experiments. In all three types of experiments the polarization production and detection efficiencies are modulated in a periodic manner. The model is also general in the sense that it applies to states with an arbitrary angular momentum F, since we used a description of the medium absorption in terms of irreducible multipole moments (here the $k = 1$ vector polarization).

Explicit expressions are given for the signal background and the resonances that occur with DC (i.e., low-pass filtered) detection as well as with phase-sensitive detection of the signal components that oscillate in-phase and in quadrature with multiples of the modulation frequency.

As a case study we have recorded the in-phase and quadrature spectra with amplitude-modulated light, detected at the first six harmonics of the modulation frequency. We find that the experimental results are well described by our model at a level of better than 5%.

We have found indications for distinct signal contributions that arise from the production and detection of atomic spin alignment (tensor polarization) that are not included in the present model. The theoretical modeling and experimental study of these alignment resonances is ongoing.

Note added. Recently, we have tested our model predictions against polarization modulation experiments. We find—as in the amplitude modulation case reported above—an excellent agreement (both for low-pass filtered and for lock-in detected signals) between experiments and model predictions. Moreover, we have observed that the relative amplitudes of all resonances (in the q and m space) are perfectly well described by the model predictions, even when the power is increased to levels that exceed the the model's range of validity by a factor of 20. It is nearly the overall amplitude of the signals that shows a saturation behavior.

ACKNOWLEDGMENTS

The authors thank P. Knowles, E. Breschi, and V. Lebedev for critical reading of the manuscript and useful comments. This work was supported by the Grant No. 200020_140421/1 of the Swiss National Science Foundation.

APPENDIX A: FOURIER STRUCTURE OF $P^{\mathrm{TOE}}(t)$

The time dependence of the transmitted power $P^{\mathrm{TOE}}(t)$ is obtained by inserting expression (37) for Γ_p

$$\Gamma_p(t) = \gamma_p \sum_{k=-\infty}^{\infty} g_k \cos(k\,\omega_{\mathrm{mod}} t) \equiv \gamma_p\, f^{\mathrm{TOE}}_{\omega_{\mathrm{mod}}}(t), \quad \text{(A1)}$$

here with summation index k instead of m, and the time-dependent polarization (41)

$$S_z^{\mathrm{TOE}}(t) = 2\,G \sum_{m=-\infty}^{\infty} g_m \left[\mathcal{A}_m(\omega_L)\cos(m\omega_{\mathrm{mod}}t) + \mathcal{D}_m(\omega_L)\sin(m\omega_{\mathrm{mod}}t)\right], \quad \text{(A2)}$$

into the general system response function (18)

$$P^{\mathrm{TOE}}(t) = A^{\mathrm{TOE}} + B^{\mathrm{TOE}}\, f^{\mathrm{TOE}}_{\omega_{\mathrm{mod}}}(t) + C^{\mathrm{TOE}}\, S_z^{\mathrm{TOE}}(t)\, f^{\mathrm{TOE}}_{\omega_{\mathrm{mod}}}(t). \quad \text{(A3)}$$

Expansion of the result yields

$$\begin{aligned}
P^{\mathrm{TOE}}(t) &= A^{\mathrm{TOE}} + B^{\mathrm{TOE}} \sum_{k=-\infty}^{\infty} g_k \cos(k\,\omega_{\mathrm{mod}}t) + 2\,C^{\mathrm{TOE}}\,G \sum_{m=-\infty}^{\infty} g_m\,\mathcal{A}_m(\omega_L)\cos(m\,\omega_{\mathrm{mod}}t) \sum_{k=-\infty}^{\infty} g_k \cos(k\,\omega_{\mathrm{mod}}t) \\
&\quad + 2\,C^{\mathrm{TOE}}\,G \sum_{m=-\infty}^{\infty} g_m\,\mathcal{D}_m(\omega_L)\sin(m\,\omega_{\mathrm{mod}}t) \sum_{k=-\infty}^{\infty} g_k \cos(k\,\omega_{\mathrm{mod}}t) \\
&= A^{\mathrm{TOE}} + B^{\mathrm{TOE}} \sum_{k=-\infty}^{\infty} g_k \cos(k\,\omega_{\mathrm{mod}}t) + G\,C^{\mathrm{TOE}} \sum_{m=-\infty}^{\infty} g_m\,\mathcal{A}_m(\omega_L) \sum_{k=-\infty}^{\infty} g_k\{\cos[(k+m)\,\omega_{\mathrm{mod}}t] \\
&\quad + \cos[(k-m)\,\omega_{\mathrm{mod}}t]\} + G\,C^{\mathrm{TOE}} \sum_{m=-\infty}^{\infty} g_m\,\mathcal{D}_m(\omega_L) \sum_{k=-\infty}^{\infty} g_k\{\sin[(k+m)\,\omega_{\mathrm{mod}}t] - \sin[(k-m)\,\omega_{\mathrm{mod}}t]\}. \quad \text{(A4)}
\end{aligned}$$

After translating the summation indices $k \rightarrow q = k + m$ and $k \rightarrow q = k - m$ of the two terms in the sums of the C^{TOE} term, and renaming the summation index k in the B^{TOE} term to q, the time-dependent power can be rewritten as

$$
\begin{aligned}
P^{\mathrm{TOE}}(t) &= A^{\mathrm{TOE}} + B^{\mathrm{TOE}} \sum_{q=-\infty}^{\infty} g_q \cos(q\,\omega_{\mathrm{mod}} t) + G\,C^{\mathrm{TOE}} \sum_{m=-\infty}^{\infty} g_m\,\mathcal{A}_m(\omega_L) \left[\sum_{q=-\infty}^{\infty} g_{q-m} \cos(q\omega_{\mathrm{mod}} t) \right. \\
&\quad \left. + \sum_{q=-\infty}^{\infty} g_{q+m} \cos(q\omega_{\mathrm{mod}} t) \right] + G\,C^{\mathrm{TOE}} \sum_{m=-\infty}^{\infty} g_m\,\mathcal{D}_m(\omega_L) \left[\sum_{q=-\infty}^{\infty} g_{q-m} \sin(q\omega_{\mathrm{mod}} t) + \sum_{q=-\infty}^{\infty} g_{q+m} \sin(q\omega_{\mathrm{mod}} t) \right] \\
&= A^{\mathrm{TOE}} + B^{\mathrm{TOE}} \sum_{q=-\infty}^{\infty} g_q \cos(q\,\omega_{\mathrm{mod}} t) + G\,C^{\mathrm{TOE}} \sum_{q=-\infty}^{\infty} \sum_{m=-\infty}^{\infty} g_m\,(g_{q-m} + g_{q+m})\,\mathcal{A}_m(\omega_L) \cos(q\omega_{\mathrm{mod}} t) \\
&\quad + G\,C^{\mathrm{TOE}} \sum_{q=-\infty}^{\infty} \sum_{m=-\infty}^{\infty} g_m\,(g_{q-m} - g_{q+m})\,\mathcal{D}_m(\omega_L) \sin(q\omega_{\mathrm{mod}} t) \\
&= A^{\mathrm{TOE}} + B^{\mathrm{TOE}}\,g_0 + \gamma_p\,C^{\mathrm{TOE}} \sum_{m=-\infty}^{\infty} g_m^2\,\mathcal{A}_m(\omega_L) + B^{\mathrm{TOE}} \sum_{\substack{q=-\infty \\ q\neq 0}}^{\infty} g_q \cos(q\,\omega_{\mathrm{mod}} t) \\
&\quad + G\,C^{\mathrm{TOE}} \sum_{\substack{q=-\infty \\ q\neq 0}}^{\infty} \sum_{m=-\infty}^{\infty} g_m\,(g_{q-m} + g_{q+m})\,\mathcal{A}_m(\omega_L) \cos(q\omega_{\mathrm{mod}} t) \\
&\quad + G\,C^{\mathrm{TOE}} \sum_{\substack{q=-\infty \\ q\neq 0}}^{\infty} \sum_{m=-\infty}^{\infty} g_m\,(g_{q-m} - g_{q+m})\,\mathcal{D}_m(\omega_L) \sin(q\omega_{\mathrm{mod}} t)\,. \qquad \text{(A5)}
\end{aligned}
$$

In the last transformation we have extracted explicitly the time-independent ($q = 0$) terms from the sums over q. Lock-in demodulation is done at frequencies $q\,\omega_L$, where q is a positive nonzero integer. As a last step, we therefore transform (A5) to have the sum over q run over positive values only,

$$
\begin{aligned}
P^{\mathrm{TOE}}(t) &\equiv A^{\mathrm{TOE}} + B^{\mathrm{TOE}}\,g_0 + G\,C^{\mathrm{TOE}} \sum_{m=-\infty}^{\infty} g_m^2\,\mathcal{A}_m(\omega_L) + 2B^{\mathrm{TOE}} \sum_{q=1}^{\infty} g_q \cos(q\,\omega_{\mathrm{mod}} t) \\
&\quad + G\,C^{\mathrm{TOE}} \sum_{q=1}^{\infty} \sum_{m=-\infty}^{\infty} g_m\,(g_{q-m} + g_{q+m} + g_{-q-m} + g_{-q+m})\,\mathcal{A}_m(\omega_L) \cos(q\omega_{\mathrm{mod}} t) \\
&\quad + G\,C^{\mathrm{TOE}} \sum_{q=1}^{\infty} \sum_{m=-\infty}^{\infty} g_m\,(g_{q-m} - g_{q+m} - (g_{-q-m} - g_{-q+m}))\,\mathcal{D}_m(\omega_L) \sin(q\omega_{\mathrm{mod}} t) \\
&= A^{\mathrm{TOE}} + B^{\mathrm{TOE}}\,g_0 + G\,C^{\mathrm{TOE}} \sum_{m=-\infty}^{\infty} g_m^2\,\mathcal{A}_m(\omega_L) + 2B^{\mathrm{TOE}} \sum_{q=1}^{\infty} g_q \cos(q\,\omega_{\mathrm{mod}} t) \\
&\quad + 2\,G\,C^{\mathrm{TOE}} \sum_{q=1}^{\infty} \sum_{m=-\infty}^{\infty} g_m\,(g_{q-m} + g_{q+m})\,\mathcal{A}_m(\omega_L) \cos(q\omega_{\mathrm{mod}} t) \\
&\quad + 2\,G\,C^{\mathrm{TOE}} \sum_{q=1}^{\infty} \sum_{m=-\infty}^{\infty} g_m\,(g_{q-m} - g_{q+m})\,\mathcal{D}_m(\omega_L) \sin(q\omega_{\mathrm{mod}} t)\,, \qquad \text{(A6)}
\end{aligned}
$$

where we have used $g_i = g_{-i}$.

1. Lock-in signals

The transmitted laser power contains a time-independent term

$$
\mathcal{B}_{\mathrm{DC}}(\omega_L) \equiv A^{\mathrm{TOE}} + B^{\mathrm{TOE}}\,g_0 + G\,C^{\mathrm{TOE}} \sum_{m=-\infty}^{\infty} g_m^2\,\mathcal{A}_m(\omega_L), \qquad \text{(A7)}
$$

in addition to the harmonic sum of all oscillating terms.

In the experiments, the time-dependent terms that oscillate in phase and in quadrature at harmonics q of the fundamental modulation frequency ω_{mod} are extracted by phase-sensitive (lock-in) detection. We recall that lock-in extraction of the in-phase and quadrature amplitudes at the qth harmonic (demodulation) consists in mixing (multiplying) the photodiode signal $P^{\mathrm{TOE}}(t)$ with $\cos(q\omega_{\mathrm{mod}} t)$ and $\sin(q\omega_{\mathrm{mod}} t)$, respectively, followed by low-pass filtering of that product. For calculational purposes, low-pass filtering is the equivalent of taking the rms time average of the mixed signal, which is equivalent to replacing $\cos(q\omega_{\mathrm{mod}} t)$ and $\sin(q\omega_{\mathrm{mod}} t)$ by $1/\sqrt{2}$ in (A6) and setting to zero the time-independent terms. Applying this procedure to the signal (A6) we obtain the

rms amplitudes of the in-phase signals following demodulation at $q\omega_{\mathrm{mod}}$

$$\frac{\mathcal{I}_{\mathrm{q}}^{\mathrm{TOE}}(\omega_L)}{\sqrt{2}} = B^{\mathrm{TOE}}\, g_q + G\, C^{\mathrm{TOE}} \times \sum_{m=-\infty}^{\infty} g_m\,(g_{q-m} + g_{q+m})\,\mathcal{A}_m(\omega_L) \qquad \text{(A8)}$$

and the corresponding quadrature amplitudes

$$\frac{\mathcal{Q}_{\mathrm{q}}^{\mathrm{TOE}}(\omega_L)}{\sqrt{2}} = G\, C^{\mathrm{TOE}} \sum_{m=-\infty}^{\infty} g_m\,(g_{q-m} - g_{q+m})\,\mathcal{D}_m(\omega_L), \qquad \text{(A9)}$$

respectively.

The structure of the resulting spectra is discussed in the body of the paper.

[1] D. Budker, W. Gawlik, D. F. Kimball, S. M. Rochester, V. V. Yashchuk, and A. Weis, Rev. Mod. Phys. **74**, 1153 (2002).

[2] D. Budker and M. Romalis, Nature Phys. **3**, 227 (2007).

[3] S. Groeger, A. Pazgalev, and A. Weis, Appl. Phys. B **80**, 645 (2005).

[4] G. Bison, N. Castagna, A. Hofer, P. Knowles, J.-L. Schenker, M. Kasprzak, H. Saudan, and A. Weis, Appl. Phys. Lett. **95**, 173701 (2009).

[5] I. Altarev *et al.*, Nucl. Instr. Meth. A **611**, 133 (2009).

[6] E. Alexandrov, M. Balabas, A. Pasgalev, A. Vershovskii, and N. Yakobson, Laser Phys. **6**, 244 (1996).

[7] S. Groeger, G. Bison, P. Knowles, R. Wynands, and A. Weis, Sensor. Actuator. Phys. **129**, 1 (2006).

[8] V. Acosta, M. P. Ledbetter, S. M. Rochester, D. Budker, D. F. Jackson Kimball, D. C. Hovde, W. Gawlik, S. Pustelny, J. Zachorowski, and V. V. Yashchuk, Phys. Rev. A **73**, 053404 (2006).

[9] W. Gawlik, L. Krzemień, S. Pustelny, D. Sangla, J. Zachorowski, M. Graf, A. O. Sushkov, and D. Budker, Appl. Phys. Lett. **88**, 131108 (2006).

[10] V. Schultze, R. IJsselsteijn, T. Scholtes, S. Woetzel, and H.-G. Meyer, Opt. Expr. **20**, 14201 (2012).

[11] W. E. Bell and A. L. Bloom, Phys. Rev. Lett. **6**, 280 (1961).

[12] W. E. Bell and A. L. Bloom, Phys. Rev. Lett. **6**, 623 (1961).

[13] E. B. Aleksandrov, Sov. Phys. Usp. **15**, 436 (1973).

[14] E. B. Alexandrov, M. Auzinsh, D. Budker, D. F. Kimball, S. M. Rochester, and V. V. Yashchuk, J. Opt. Soc. Am. B **22**, 7 (2005).

[15] A. Ben-Kish and M. V. Romalis, Phys. Rev. Lett. **105**, 193601 (2010).

[16] Y. P. Malakyan, S. M. Rochester, D. Budker, D. F. Kimball, and V. V. Yashchuk, Phys. Rev. A **69**, 013817 (2004).

[17] A. Nagel, L. Graf, A. Naumov, E. Mariotti, V. Biancalana, D. Meschede, and R. Wynands, Europhys. Lett. **44**, 31 (1998).

[18] R. Wynands, A. Nagel, S. Brandt, D. Meschede, and A. Weis, Phys. Rev. A **58**, 196 (1998).

[19] G. Alzetta, A. Gozzini, L. Moi, and G. Orriols, Nuovo Cimento B **36**, 5 (1976).

[20] I. Wolfram Research, MATHEMATICA, version 8.0 ed. (Wolfram Research, Inc., Champaign, Illinois, 2010).

[21] N. Castagna and A. Weis, Phys. Rev. A **84**, 053421 (2011).

[22] N. Castagna, G. Bison, G. Domenico, A. Hofer, P. Knowles, C. Macchione, H. Saudan, and A. Weis, Appl. Phys. B **96**, 763 (2009).